J. Phys. D: Appl. Phys. **29** (1996) 753–760. Printed in the UK

A study of the convective flow as a function of external parameters in high-pressure mercury lamps

K Charrada†, G Zissis† and M Stambouli‡

† Centre de physique des Plasmas et de leurs Applications de Toulouse, 118 route de Narbonne, F-31062 Toulouse, France
‡ Ecole Normal Supérieur d'Enseignement Technique, 5 Avenue Taha Hussein, 1008 Tunis, Tunisia

Received 26 June 1995, in final form 15 October 1995

Abstract. This paper deals with the modelling of the convection processes in high-pressure mercury arcs. Temperature and velocity fields have been calculated by using a 2D semi-implicit finite-element scheme for the solution of conservation equations relative to mass, momentum and energy. After validation, this model was applied to the study of the influence of arc external parameters such as mercury charge and tube diameter on the convective processes. It was found that stable laminar mono-cellular convection flow occurs at low values of tube diameter for a cylindrical burner and/or a low mercury charge. Finally, we considered in detail the region behind the electrodes, where an accumulation of mercury is observed. The evaluation of this amount of mercury 'trapped' in these regions is of prime importance for a good description of the distribution of mercury in the burner and for a correct evaluation of the total discharge pressure.

1. Introduction

Transport phenomena in electric arcs are responsible for effects of considerable importance to stable operation of the device. If the convection flow is unstable, undesirable phenomena appear and several discharge characteristics are affected. Elenbaas (1951) and Kenty (1938) interpreted such instabilities observed at sufficiently high pressure as a transition from laminar to turbulent convective flow at high convective velocities. However, Zollweg (1977) believed that the instability of mercury arcs can be explained as a helical instability resulting from the self-magnetization of the arc.

Modelling of the convection processes in high-pressure mercury arcs has been discussed in numerous papers including those of Zollweg (1978), Lowke (1979) and Chang *et al* (1990). However, to the author's knowledge, there is no precise quantitative description of the effect of mass transport on the high-pressure mercury lamp, neither in these papers nor in other references. Moreover, except for a short paper of Weber (1986) dealing with an experimental mapping of Hg and Xe densities in high-pressure lamps, we looked in vain, in the literature, for an accurate verification of the amount of mercury distributed in the three different discharge zones: the regions above and behind respectively the lower and higher electrodes, and the inter-electrode volume. Obviously, the discharge occurs practically in the region between the electrodes. So, only the amount of mercury in this zone is considered to be the active part of the total amount of mercury introduced into the burner. Mercury accumulated in the other regions can be considered as a mercury loss. Anyway, we cannot eliminate this loss. However, a good evaluation of the amount of mercury 'trapped' in these regions is of prime importance for a good description of the mercury distribution in the burner and for a correct determination of the total discharge pressure.

In the case of an atmospheric pressure discharge the flow is highly dependent on the total amount of mercury and the current as well as on the arc tube dimensions. In fact, in high-pressure lamps these parameters are linked to practical constraints related to wall loading and arc tube voltage. However, in this paper we neglect these constraints and we consider these quantities to be completely independent of each other. This assumption will allow us to study a large range of mercury loadings and arc tube radii in order to evaluate their relative importance. Furthermore, we focus much attention on the region behind the electrodes, where an accumulation of mercury is observed. This simulation of arc properties is performed with a 2D code. Mass, energy and momentum continuity equations are solved in order to calculate transport flows. Numerical resolution is achieved by using a finite-element semi-implicit scheme. In order to confirm the validity of the model adopted for this study, a comparison is made with measurements and calculations of other authors.

0022-3727/96/030753+08$19.50

2. Description of the model

2.1. Basic assumptions

We assume an axially symmetric arc in local thermodynamic equilibrium (LTE) and at steady state. Under such assumptions, all discharge properties can be deduced from the temperature distribution. Thus, the required material functions, namely thermal and electric conductivity, specific heat of arc plasma and net emission coefficient, are assumed to be fully described in terms of the local temperature only. It is also assumed that the plasma flow is laminar and that the electrodes are of cylindrical shape. In this work all phenomena at the electrode surface and electrode regions are omitted. Thus our model results can be considered to be valid a few mean free paths distant from the electrodes. We also neglect the viscous energy dissipation and we suppose that the electric field is purely axial. We assume that the contribution of magnetic force is negligible.

2.2. The governing equations

Under these conditions, the positive column plasma is governed by usual balance equations concerning mass, radial momentum, axial momentum and energy conservation. These equations in cylindrical coordinates (r and z) are as follows.

For mass conservation

$$\frac{1}{r}\frac{\partial}{\partial r}(r\rho v_r) + \frac{\partial}{\partial z}(\rho v_z) = 0. \tag{1}$$

For radial momentum conservation

$$v_r\frac{\partial v_r}{\partial r} + v_z\frac{\partial v_r}{\partial z} = -\frac{1}{\rho}\frac{\partial p}{\partial r} + \frac{1}{\rho}\left[\frac{1}{r}\frac{\partial}{\partial r}\left(r\eta\frac{\partial v_r}{\partial r}\right) + \frac{\partial}{\partial z}\left(\eta\frac{\partial v_r}{\partial z}\right) - 2\eta\frac{v_r}{r^2}\right]. \tag{2}$$

For axial momentum conservation

$$v_r\frac{\partial v_z}{\partial r} + v_z\frac{\partial v_z}{\partial z} = -\frac{1}{\rho}\frac{\partial p}{\partial z} - g + \frac{1}{\rho}\left[\frac{1}{r}\frac{\partial}{\partial r}\left(r\eta\frac{\partial v_z}{\partial r}\right) + \frac{\partial}{\partial z}\left(\eta\frac{\partial v_z}{\partial z}\right)\right]. \tag{3}$$

For energy conservation

$$\rho c_p\left(v_r\frac{\partial T}{\partial r} + v_z\frac{\partial T}{\partial z}\right) = \sigma E^2 - U + \left[\frac{1}{r}\frac{\partial}{\partial r}\left(r\kappa\frac{\partial T}{\partial r}\right) + \frac{\partial}{\partial z}\left(\kappa\frac{\partial T}{\partial z}\right)\right]. \tag{4}$$

One also has the ideal gas law

$$p = \frac{R}{M}\rho T \tag{5}$$

and Ohm's law

$$I = 2\pi Eq\int_0^{R_w} r\sigma\,\mathrm{d}r. \tag{6}$$

The basic variables defined by these equations are density ρ, axial velocity v_z, radial velocity v_r, temperature T and pressure p. The plasma material functions are viscosity η, specific heat c_p, net radiative emission U, electrical conductivity σ and thermal conductivity κ. All these material functions are supposed to be functions of temperature. Other quantities of these equations are electric field E, gravity g, tube radius R_w, electric current I, elementary charge q, atomic mass M and the ideal gas constant R.

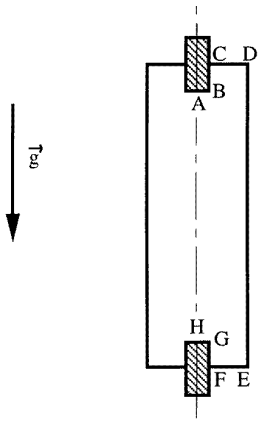

Figure 1. Boundary conditions.

We note that the contribution of the energy transfer due to the velocities of electron flow was neglected in the energy balance equation (4). The effect of this term in the central region is small, because in this region temperature gradients are relatively small. It does have an effect in the region of the arc near the cathode, where temperature gradients are relatively large. According to Lowke *et al* (1992), because this term gives a cooling effect for this region of the arc where they expect a heating effect due to the electron temperature being higher than the neutral gas temperature, it is better to omit the term.

Electric conductivity, thermal conductivity and viscosity included in this model are calculated by using the first approximation of the gas kinetic theory as developed by Hirchfelder *et al* (1954) assuming a Maxwellian shape for the electron energy distribution function and the Lennard-Jones interatomic potential. The value corresponding to a monatomic ideal gas is used for c_p (Chase *et al* 1986). Finally, the net emission coefficient is calculated according to Stormberg and Schäfer (1983). This coefficient includes UV and visible lines as well as continuum emission from the plasma. It is established for a parabolic radial temperature profile. In this work we used an interpolation to determine the net emission coefficient for a non-parabolic radial profile.

2.3. Boundary conditions

The boundary conditions are taken to be similar to those of Lowke (1979). They are summarized with reference to figure 1, in table 1.

The experimental value, T_w, corresponding to a 400 W commercial mercury discharge is taken for the wall temperature (equal to 1000 K). We also suppose that this value does not vary much with power supply. This is

Table 1. Boundary conditions.

	AH	CDEF	FG and BC	HG and AB
v_r	$v_r = 0$	$v_r = 0$	$v_r = 0$	$v_r = 0$
v_z	$\frac{\partial v_z}{\partial r} = 0$	$v_z = 0$	$v_z = 0$	$v_z = 0$
T	$\frac{\partial T}{\partial r} = 0$	$T = T_w$	$T = T(z)$	$T = T_{elc}$

Table 2. Discharge characteristics used by Zollweg and Kenty.

Parameter	Zollweg	Kenty
Arc tube length (mm)	90	$\simeq$ 170
Inter-electrode length (mm)	70	155
Internal diameter (mm)	18	33.3
Electrode length (mm)	10	$\simeq$ 7.5
Electrode diameter (mm)	2	$\simeq$ 5
Pressure (atm)	2.89	1.2
Current (A)	3.0	2.9
Hg loading (mg cm^{-1})	5.72	11.5

confirmed by using an optical pyrometer and measuring the wall temperature of a large number of lamps (it is found that wall temperature is almost constant within a limit of $\Delta T_w = \pm 200$ K. Moreover, the wall temperature is not constant along the wall; it is higher at the top than at the bottom. An accurate calculation of this temperature needs a resolution of the energy balance equation near the tube wall. Note that, in spite of the simple appearance of this equation, a rigorous evaluation of this term may be very difficult. For electrode temperature (T_{elc}) we have taken a value of 2000 K.

2.4. The numerical procedure

The partial differential equations (1)–(4) are solved by using a finite-element scheme based on rectangular structured elements and a variable step grid. The code has been checked for numerical diffusion effects; in all cases tested no significant systematic error was detected. The calculation procedure, described in more detail elsewhere (Charrada 1995), is outlined as follows:

(i) rectangular grid generation,

(ii) initial arbitrary values of T, v_r, v_z and p are selected throughout the whole region,

(iii) all material functions are evaluated for each node,

(iv) for a given current the electric field value is calculated from Ohm's law (equation (6)),

(v) radial and axial components of convective velocity and pressure are obtained from equations (1)–(3),

(vi) new values for temperature are obtained by using equation (4) and

(vii) the procedure is repeated from step (iii) until convergence.

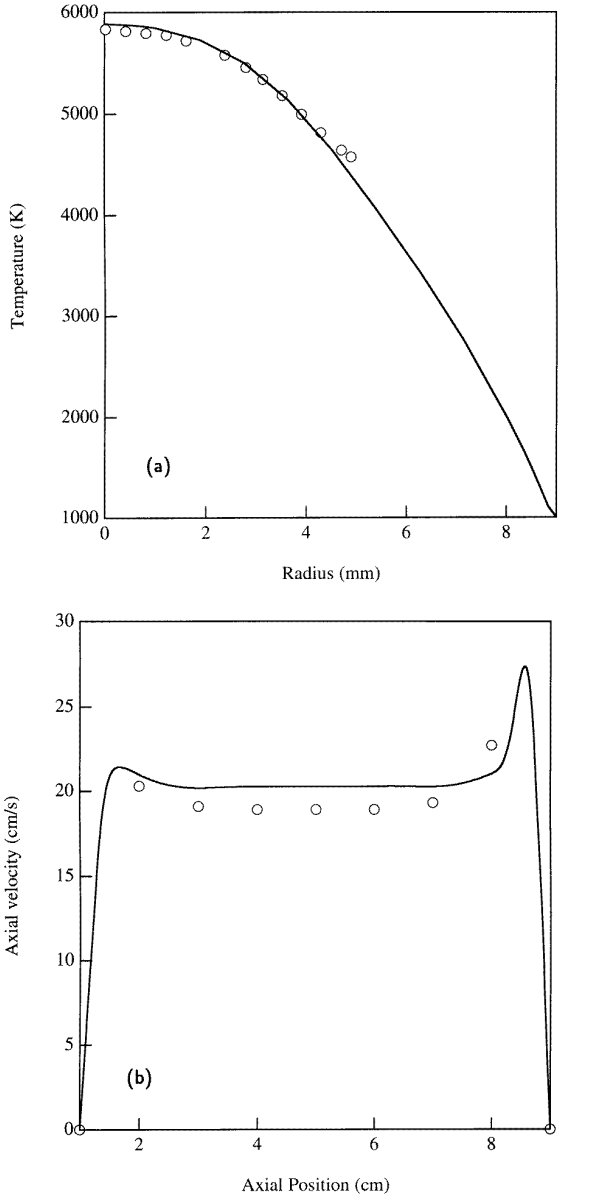

Figure 2. (*a*) A comparison between calculated (full line) and measured (symbols) temperature radial profiles. (*b*) The calculated axial velocity distribution on the arc axis; symbols denote results from Zollweg's calculations.

3. Results and discussion

3.1. Model validation

In order to confirm the validity of the model, we compared our calculations with measurements given by other authors. Here we only show the comparison between our calculations and the results of Zollweg (1978) and Kenty (1938) in the case of high-pressure mercury discharges (characteristics given in table 2).

Figure 2(*a*) shows the experimental data and our calculation results concerning the temperature profile for the middle cross section of the positive column. We note the good agreement between our calculation results and experimental results. Figure 2(*b*) gives our results for axial

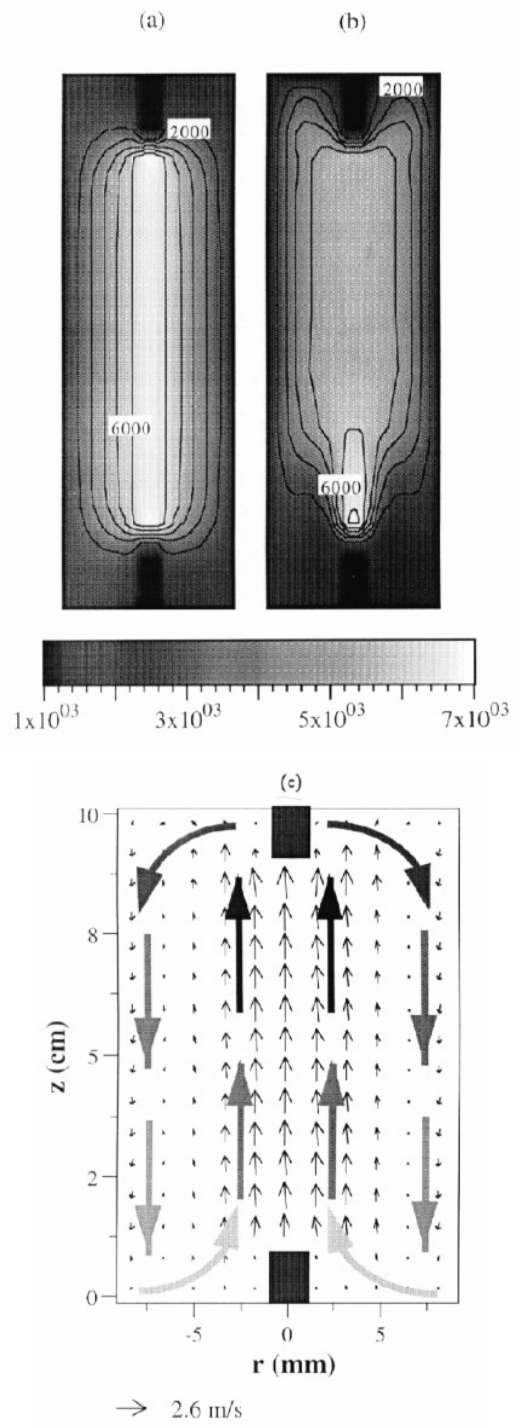

Figure 3. The calculated temperature field for two different amounts of mercury: (*a*) m_{Hg} = 10 mg and (*b*) m_{Hg} = 200 mg. (*c*) The calculated map of the velocity vectors in the discharge vessel. Thick arrows illustrate qualitatively the convection pattern. Note that the arrow grey level is in relation to the gas temperature (the blacker the arrow the hotter the gas).

velocity distribution on the axis. Zollweg's calculations (Zollweg 1978) are also included in the same plot. The agreement between these two sets of results is found to be satisfactory. The small difference between them can be explained in terms of differences between numerical methods and different approaches used for the evaluation of the plasma material functions.

As reported by Kenty, the upward convective velocity in the centre of the middle plane of the arc tube is of the order of 40 cm s^{-1}; the calculations of Chang and Dakin (1991) confirms this value. In the case of a similar discharge we obtain from our numerical code a value of 38 cm s^{-1}, which is in acceptable agreement with the above values. This result is also in good agreement with the empirical relation v_z (cm s^{-1})= $5m^{0.85}$ (mg cm^{-1}) given by Fohl (1975).

3.2. Study of the influence of the total amount of mercury

In this study the DC current value is maintained at 3.2 A. The burner has an electrode spacing of 7.2 cm with a total length of 9.2 cm. The arc tube diameter is 1.85 cm. The 1 cm long electrodes have a radius of 0.1 cm. These characteristics of the electrodes have been taken the same for all cases studied in this paper. The amount of mercury in the burner is taken in the range 10–200 mg, varying in steps of 10 mg.

The calculated temperature distributions for the two extreme amount of mercury (10 and 200 mg) are shown in figures 3(*a*) and (*b*) respectively. Constriction at the lower electrode increases when the amount of mercury rises. We also remark that increasing the total mercury mass in the discharge leads to the heating of the zone behind the higher electrode. This is explained by the fact that the gas on the tube axis is heated because it is at the core of the arc where the gas near the wall is cooled by conduction. The density difference between the gas at the core and that at the arc periphery establishes an upwind flow in the centre and a downwind flow adjacent to the wall. Thus, the hot gas coming out of the arc channel heats the region behind the upper electrode. Figure 3(*c*) illustrates this convective flow in the discharge vessel. The arc constriction in the lower electrode region is caused by the cold gas from the arc periphery coming back into the hot central channel.

The radial thermal fluxes in the median plane for increasing mercury amounts from 10 to 190 mg (by steps of 20 mg) are plotted in figure 4. One can see that, when the amount of mercury increases, the radial thermal flux decreases in the core of the arc and rises in the periphery. This phenomenon is due to the arc broadening with increasing total amount of mercury in the burner. The corresponding thermal conduction loss as a function of the amount of mercury is shown in figure 5. We note that the axial thermal conduction can be neglected (Charrada 1995).

Convective transport of energy to the tube wall was found to be insignificant compared to other kinds of losses, for the amounts of mercury studied here. Figure 6 shows the variation of the power loss by convection versus the square of the amount of mercury. It is clearly shown that this loss is not important even for 200 mg of mercury. Nevertheless, convective flows in arcs are responsible for considerably important effects concerning operating device stability.

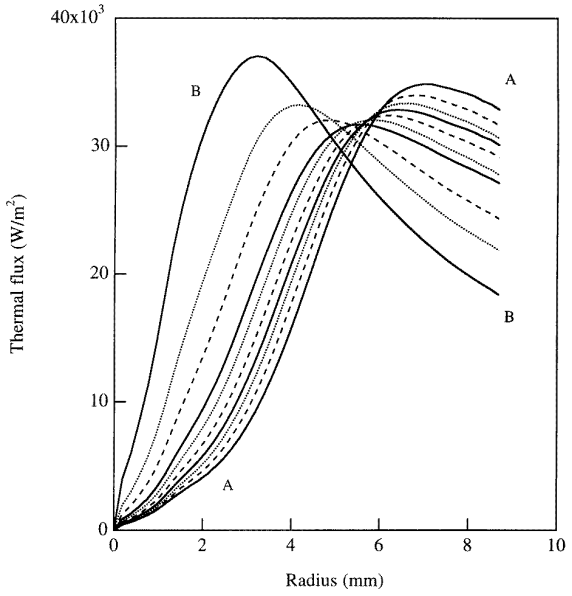

Figure 4. The radial component of thermal flux versus the amount of mercury in the burner; the amount of mercury was varied from 10 mg (curve B) to 190 mg (curve A) by steps of 20 mg.

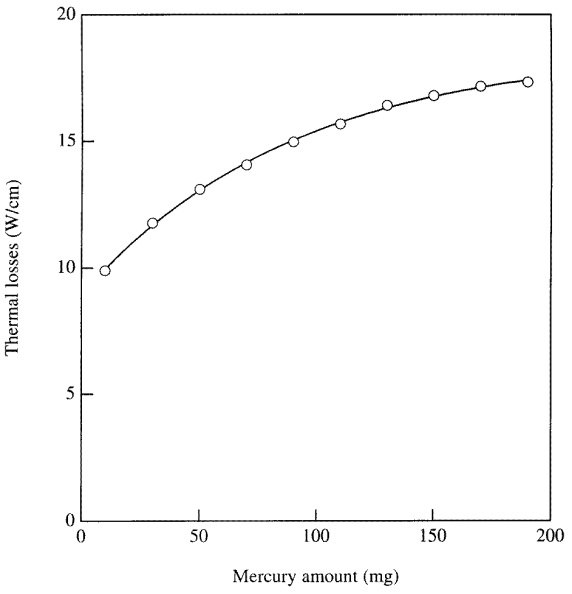

Figure 5. Energy losses due to radial conduction as a function of the amount of mercury.

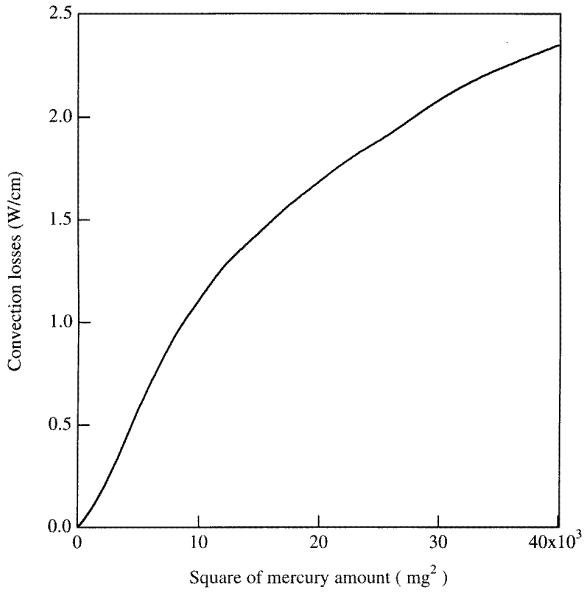

Figure 6. Energy losses due to convection as a function of the amount of mercury.

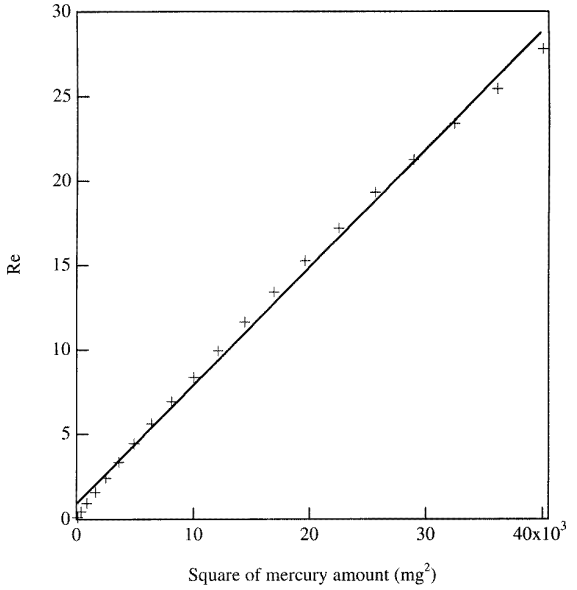

Figure 7. The Reynolds number as a function of the amount of mercury.

As shown previously in figure 3(*b*), a mono-cellular convection pattern appears in the discharge vessel. The transition from laminar to turbulent flow is characterized by a critical value of 1400 for the Reynolds number (Elenbaas 1951). The mean value of the latter, calculated as in equation (7), is given in figure 7 as a function of the square of the mass:

$$\mathrm{Re} = \frac{2}{R}\int_0^R r\frac{\rho v}{\eta}\,\mathrm{d}r. \qquad (7)$$

The variation in Re versus the amount of mercury is approximated by $c_1 + c_2 m_{Hg}^2$, with c_1 and c_2 constants equal to 0.9 and 7×10^{-4} mg^{-2} respectively. If the validity of this formula is extrapolated to give values for amounts of mercury that we have not yet examined, the flow becomes turbulent for unit length mercury mass greater than 150 mg cm^{-1}

It is very important to know how the amount of mercury, initially introduced as a liquid into the burner, will be distributed over the three main discharge zones cited in the introduction of this paper. This distribution is a result of the temperature profile in the plasma. As we have stated, the hot gas coming out of the arc channel heats the region behind the upper electrode. Thus, there should

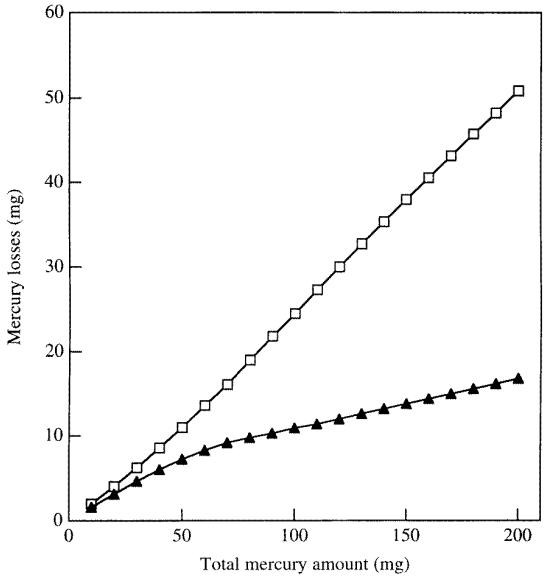

Figure 8. The variation in the amount of mercury trapped in the electrode regions as a function of the total amount of mercury: (▲), higher electrode region and (□), lower electrode region.

be less mercury accumulated in this region than behind the lower one. The mass of mercury accumulated in the regions behind each electrode as a function of the total amount of mercury in the burner is given in figure 8.

3.3. A study of the influence of the tube diameter

In this study the current value is maintained at 3 A and the mercury pressure is 3 atm. The confining tube has an electrode spacing of 5 cm for a total length of 7 cm. The arc tube diameter is made to vary in the range 1–3 cm by steps of 0.5 cm.

In figure 9 we draw the calculated temperature distributions for the two extreme arc tube diameters (1 and 3 cm). Here also constriction at the lower electrode increases when the arc tube radius increases (the same phenomenon has been observed when the amount of mercury increases at constant electric current and geometry).

Convective effects are responsible for this constriction. For a small arc tube radius the convection hardly exists, but when the radius becomes high enough, convection does play an important role. So, it leads to an asymmetry on either side of the median discharge plane (the horizontal plane midway between the electrodes).

Figure 10 illustrates the effect of mass transport upon radial thermal flux in the median plane. We can observe the decrease of this quantity near the wall when the radius increases. Note that the thermal energy losses are practically proportional to the radial thermal flux at the wall. So when the tube radius increases, convection tends to thermalize the peripheral region of the plasma. Thus, the temperature gradient near the wall decreases in turn hence leading to a decrease in the thermal losses. Moreover, when

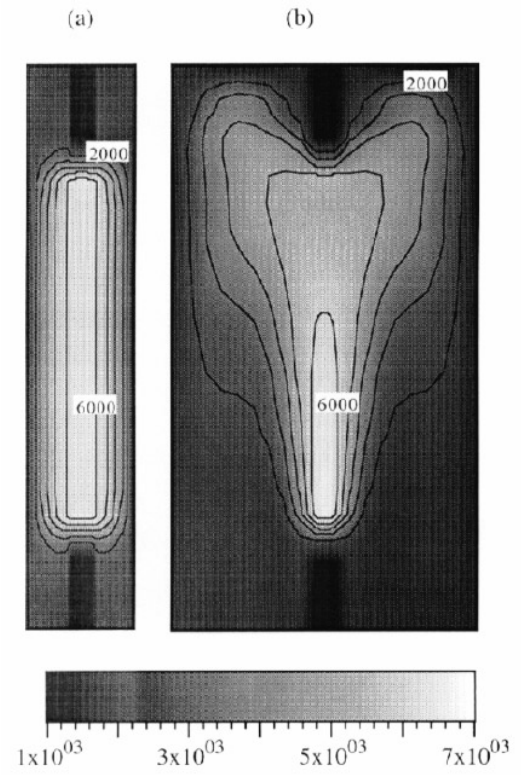

Figure 9. The calculated temperature field for two different arc tube diameters: (*a*) d = 1 cm and (*b*) d = 3 cm.

the radius becomes sufficiently high, the arc shows a free-burning character (Lowke 1979). This observation can be illustrated by figure 11 which shows the temperature profile for different arc tube diameters. It is clearly shown that the temperature profile in the case of 3 cm arc tube diameter is quite similar to that of a free-burning arc.

In figure 12 we give the Reynolds number calculated by our model as a function of arc tube diameter. This variation can be approximated by $c_3 d^4$, where c_3 is a constant equal to 0.557 cm^{-4} and d is the tube diameter in centimetres. Again, if we assume that this formula remains valid for higher arc tube diameters, the flow becomes turbulent for an arc tube diameter value of 7 cm.

The amount of mercury accumulated in the regions behind both electrodes as a function of the square of arc tube diameter is given in figure 13. We observe that an increase in arc tube diameter leads to an increase in the amount of mercury in these regions. So, a small radius leads to a reduction in this mercury loss. However, the arc tube radius should be high enough to keep the thermal loss relatively low.

4. Conclusion

The aim of this paper was to study the influence of arc external parameters on transport phenomena resulting in convection flow in high-pressure mercury discharge lamps. After validation, the retained model was applied to the description of the high-pressure mercury discharge.

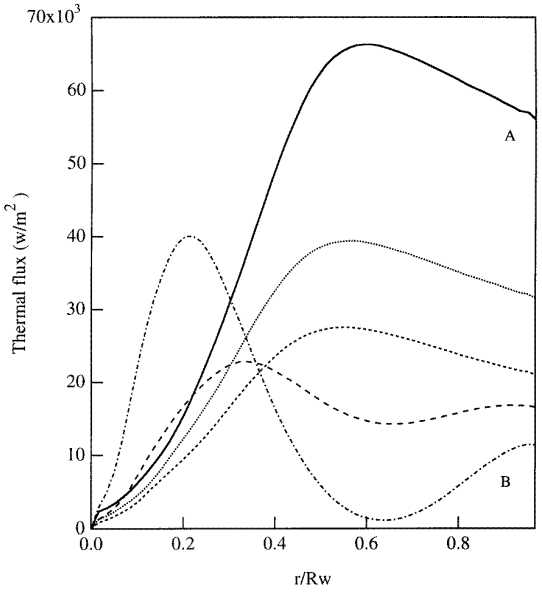

Figure 10. The radial component of thermal flux versus tube diameter; the tube diameter was varied from d = 1 cm (curve A) to d = 3 cm (curve B) by steps of 0.5 cm.

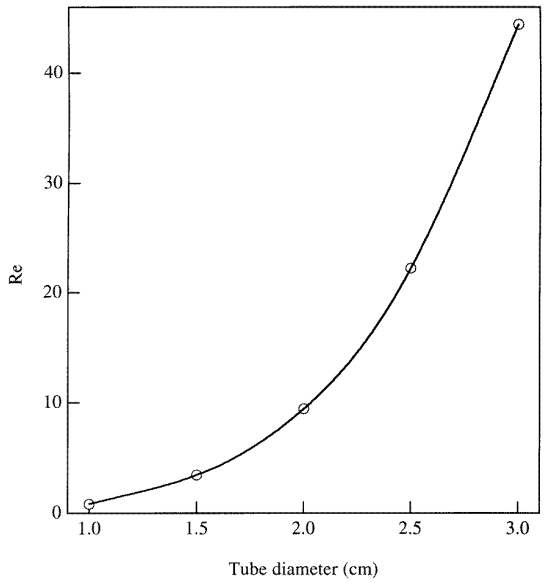

Figure 12. The Reynolds number as a function of the tube diameter.

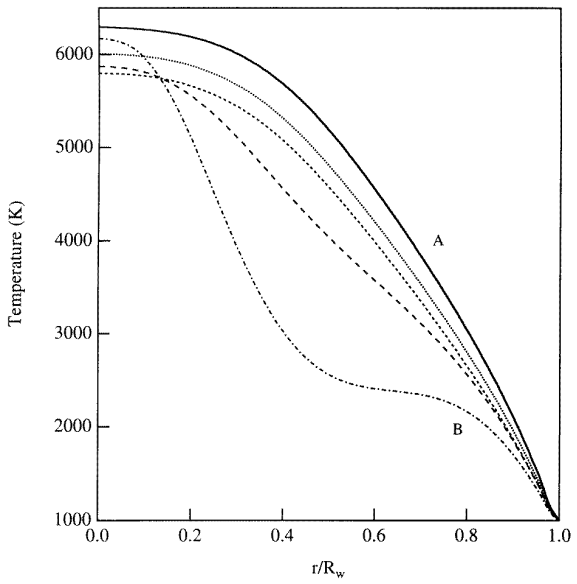

Figure 11. The dependence of the temperature profile upon the tube diameter; the tube diameter was varied from d = 1 cm (curve A) to d = 3 cm (curve B) by steps of 0.5 cm.

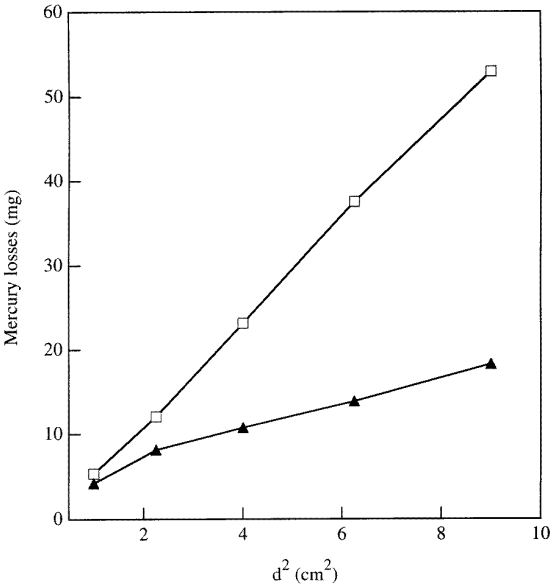

Figure 13. The variation in the amount of mercury trapped in the electrode regions as a function of the tube diameter: (▲), higher electrode region and (□), lower electrode region.

It was found that stable laminar mono-cellular convection flow occurs at low values of tube diameter for a cylindrical burner and/or a low mercury charge. However, as is known, the Reynolds number increases with tube diameter and/or mercury pressure, thus a turbulent flow will appear up to a critical value ($m_{Hg}^{cr} = 150$ mg/cm and $R^{cr} = 7$ cm). In the proximity of this critical value, a more complex multi-cellular convection flow pattern may occur (Fohl 1975). In the case of a wall-stabilized discharge the convection losses are a small fraction of the total amount of energy in the discharge. However, it is recognized that, in some cases, convection could affect some discharge performances. Finally, we focused much attention on the region behind the electrodes where an accumulation of mercury is observed. The evaluation of this amount of mercury 'trapped' in these regions is of prime importance for a good description of the mercury distribution in the burner and for a correct evaluation of total discharge pressure.

Acknowledgments

The authors are indebted to Professor J J Damelincourt for numerous discussions on this subject. They would also like to thank N Sewraj. This work was partially supported by the EDF 'Club Arc'.

References

Chang P Y and Dakin J T 1991 *J. Appl. Phys.* **69** 3763–5
Chang P Y, Shyy W and Dakin J T 1990 *Int. J. Heat Mass Transfer* **15** 51
Charrada K 1995 *Thèse du Doctorat* l'Université Paul Sabatier, Toulouse
Chase M W, Davies C A Jr, Downey J R, Frurip D Jr, McDonald R A and Syverud A N 1986 *JANAF Thermochemical Tables* (New York: American Chemical Society and American Institute of Physics)
Elenbaas W 1951 *The High Pressure Mercury Vapour Discharge* (Amsterdam: North Holland)
Fohl T 1975 *J. IES* July 265–70
Hirschfelder J O, Curtiss C F and Bird R B 1954 *Molecular Theory of Gases and Liquids* (New York: Wiley)
Kenty C 1938 *J. Appl. Phys.* **9** 53–66
Lowke J J 1979 *J. Appl. Phys.* **50** 147–57
Lowke J J, Kovitya P and Schmidt H P 1992 *J. Phys. D: Appl. Phys.* **25** 1600–6
Stormberg H P and Schäfer R 1983 *J. Appl. Phys.* **54** 4338–47
Weber B 1986 *Proc. 4th Int. Symp. on the Science and Technology of Light Sources* (Karlsruhe: Universität Karlsruhe) pp 225–6
Zollweg R J 1977 *Bull. Am. Phys. Soc.* **22** 197
——1978 *J. Appl. Phys.* **49** 1077–91